Molecular Conformation Modulating Luminescence Switching between Delayed Fluorescence and Room-Temperature Phosphorescence

Yating Wen [a], Shengbing Xiao [a], Haichao Liu *[a], Xuzhou Tian [a], Jianbo De [b], Tong Lu [a], Zhiqiang Yang [a], Deyue Zou [cd], Ying Lv [c], Shi-Tong Zhang [a], Qing Su [e], and Bing Yang *[a]

[a.] State Key Laboratory of Supramolecular Structure and Materials, College of Chemistry, Jilin University, Changchun 130012 (P.R. China). E-mail: hcliu@jlu.edu.cn; yangbing@jlu.edu.cn

[b.] Beijing Key Laboratory for Optical Materials and Photonic Devices, Department of Chemistry, Capital Normal University, Beijing 300072 (P.R. China)

[c.] State Key Laboratory of Luminescence and Applications, Changchun Institute of Optics, Fine Mechanics and Physics, Chinese Academy of Sciences, Changchun 130033 (P.R. China).

[d.] University of Chinese Academy of Sciences, Beijing 100049, (P.R. China).

[e.] College of Chemistry, Jilin University, Changchun 130012 (P.R. China).

SI-1. Experimental procedures

General information: All reactants and solvents were purchased from commercial sources, and used without further purification. The synthesis procedure was presented in Scheme S1. ^{1}H and ^{13}C NMR spectra were recorded on WNMR-I 400, using tetramethylsilane (TMS) as the internal standard. The MALDI-TOF-MS mass spectra were recorded using an AXIMA-CFR^{TM} plus instrument. The compounds were characterized by a Flash EA 1112, CHNS elemental analysis instrument.

The synthesis of p-chlorobenzoyl-iminostilbene (IS-CBZ)

1 ml triethylamine (TEA) was added to a dichloromethane solution of iminostilbene (2.82 mmol) and stirred overnight. Subsequently, *p*-chlorobenzoyl chloride (5.64 mmol) was dropped to the mixture and stirred for 2 hours at room temperature (RT). The mixture was poured into 50 mL petroleum ether, and filtrated. The residue was purified by silica gel column chromatography using dichloromethane as eluent to afford IS-CBZ as white solid. The yield is 68%. ^{1}H NMR (400 MHz, CD$_2$Cl$_2$, CF$_3$COOD, 25 °C, TMS): δ = 7.67 (d, J = 7.9 Hz, 1H), 7.59 (dd, J = 17.1, 7.9 Hz, 2H), 7.48 (dd, J = 17.8, 7.6 Hz, 2H), 7.34 (t, J = 7.5 Hz, 1H), 7.28 – 7.15 (m, 7H), 7.08 (d, J = 7.9 Hz, 1H). ^{13}C NMR (101 MHz, CD$_2$Cl$_2$, CF$_3$COOD, 25 °C, TMS): δ = 172.58, 139.44, 137.77, 136.85, 134.25, 133.25, 131.46, 129.65, 129.53, 129.44, 129.38, 129.23, 128.53, 128.42, 127.55, 127.29. MALDI-TOF MS (mass *m/z*): [*M*$^+$] Calcd (%) for C$_{21}$H$_{14}$NClO, 331.1; Found: 330.93. Anal. Calcd for C$_{21}$H$_{14}$NClO: C 76.02, H 4.25, O 4.82, N 4.22; found: C 76.20, H 4.26, O 4.88, N 4.20.
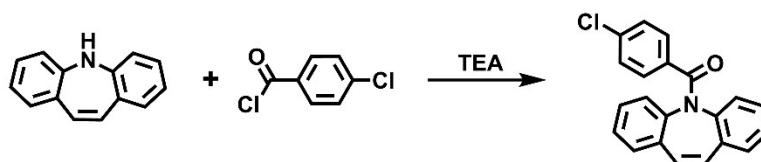
Scheme S1. Synthesis route of IS-CBZ.

Photophysical measurements: UV–vis absorption spectra were recorded on a Shimadzu UV-3100 Spectrophotometer. Photoluminescence (PL) spectra and lifetimes were carried out on a FLS980 Spectrometer. Solid-state photoluminescence quantum efficiency (PLQY) was measured with an integrating sphere, and the excitation wavelength is 310 nm. Temperature-dependent PL spectra and temperature-dependent time-resolved PL spectra were collected by using the programmed temperature method on a FLS980 Spectrometer, and the excitation wavelength is 330 nm. The crystals were fixed on the quartz plate in terms of spectra and lifetimes. For the pulse pumping experiments, the excitation source was a pulsed CryLaS FTSS355-50 solid-state laser system with a repetition rate of 50 Hz and a pulse duration of 1.0 ns, emitting at 355 nm. A cylindrical lens was used to shape the laser beam into a stripe with an estimated width of 200 um and long of 2 mm. The maximum output energy of the laser is 150 uJ. Excitation pulse energies are adjusted by a circular gradient density neutral filter and recorded using an energy meter (EnergyMax-USB J-10SI-HE, Coherent, USA). The output wavelength is monitored by a high-resolution fiber optic spectrometer (AvaSpec-ULS3648-USB2-UA-25, Avantes, Netherlands).

The measuring unit of the spectrophotometer is based on the AvaBench75 platform with a Czerny-Turner optical bench and 3648 element CDD detector matrix. The dynamic range of the detector matrix (the signal to noise ratio) was ~50 dB. The detector of the spectrophotometer had a coating enhancing the sensitivity of the matrix in the ultraviolet range. Collector lenses of the detector additionally enhanced the sensitivity of measurements.

Single crystal X-ray diffraction (XRD) data: B-crystal was obtained by sublimation. Y-crystal was obtained from dichloromethane solution by solvent evaporation method at room temperature (RT). The XRD data were collected with a Rigaku R-AXIS RAPID diffractometer equipped with a Mo-Kα and control Software using the RAPID AUTO at 293 (±2) K. The crystal structures were solved with a SHELXTL software. Powder XRD (PXRD) patterns were collected on a Rigaku SmartLab(3) diffractometer.

Theoretical calculation: All the density functional theory (DFT) calculations were carried out using Gaussian 09 (version D.01) package on a PowerLeader cluster.[1] The ground-state geometry was fully optimized using DFT at the level of B3LYP/6-31G (d, p). Theoretical calculations based on the time-dependent density functional theory (TD−DFT) with Tamm−Dancoff approximation using the B3LYP/6-31G (d, p) were performed for excited state energy levels and natural transition orbitals (NTOs). The molecular models were selected from the single crystal structures. The spin-orbit coupling (SOC) coefficients were quantitatively estimated at the level of B3LYP/6-31G (d, p) by Beijing density function (BDF) program.[2-5]

Thermal stability measurements: Differential scanning calorimetry (DSC) analysis was carried out using a NETZSCH (DSC-204) instrument at 10 °C min⁻¹ while flushing with nitrogen.
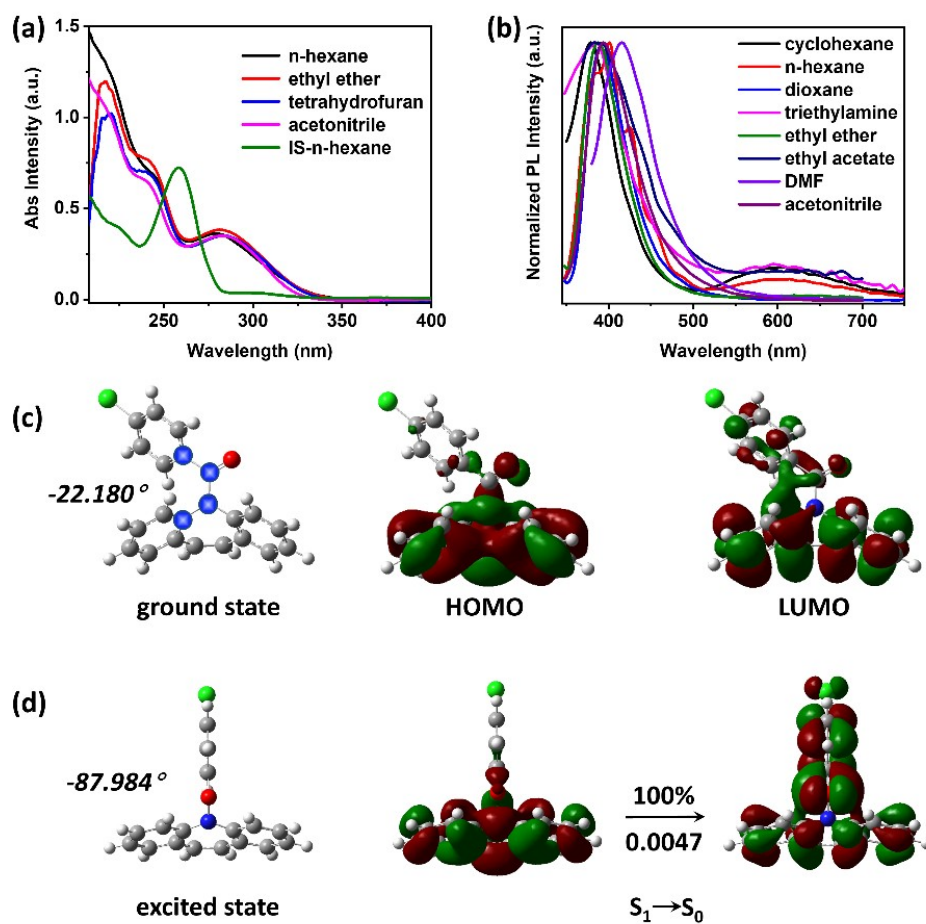
SI-2. Figures

Figure S1. (a) Absorption spectra of IS and IS-CBZ in solvents with different polarities (the concentration is $3×10^{-5}$ mol·L^{-1}). (b) Solvatochromic PL spectra of IS-CBZ with increasing polarity of solvents. (c) Optimized ground-state geometry, the highest occupied molecular orbital (HOMO), and the lowest unoccupied molecular orbital (LUMO) distributions of IS-CBZ. (d) Optimized excited-state geometry and natural transition orbitals (NTOs) for S_1 to S_0.
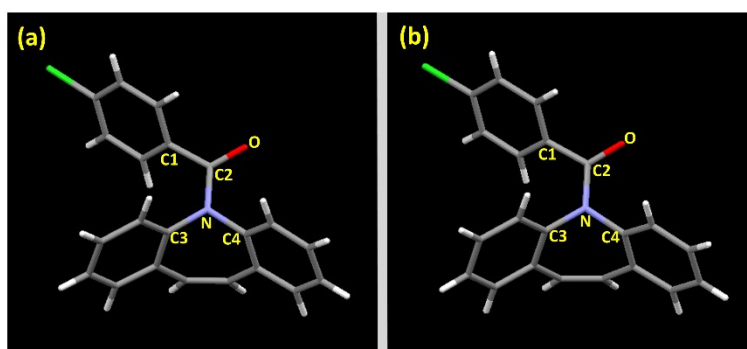
Figure S2. Different molecular conformations of IS-CBZ in (a) B-crystal and (b) Y-crystal. The bond lengths and twist angles of single-molecule conformations in crystals are listed in Table S2.
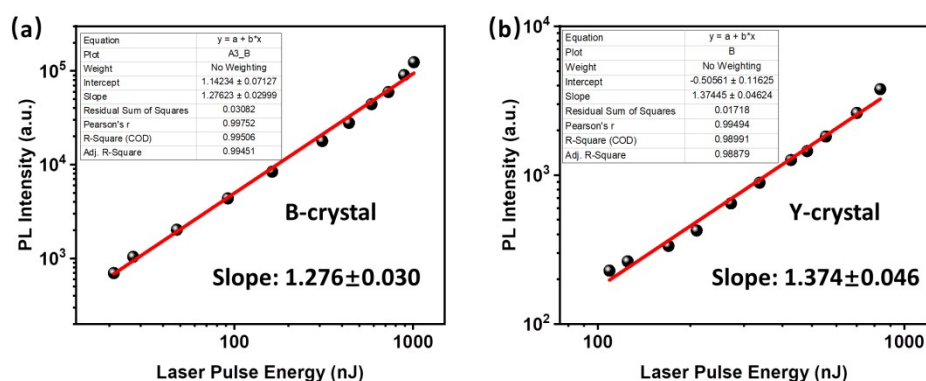
Figure S3. Double logarithmic plot of PL intensity measured as a function of laser pulse energy of (a) B-crystal and (b) Y-crystal of IS-CBZ. The PL intensity was monitored at 398 nm.

In order to distinguish the triplet-triplet annihilation (TTA) and thermally activated delayed fluorescence (TADF) mechanisms, we collected the PL spectra of samples under different excitation powers. Then the double-logarithmic relationship between the PL intensity and excitation powder was fitted. As shown in Figure S3, the B-crystal and Y-crystal of IS-CBZ showed a slope between 1 and 2, which verifies the presence of TTA. [6] Employing an exclusive method, if the luminescence mechanism is one of the prompt fluorescence (PF), TADF and room-temperature phosphorescence (RTP), the slope of double-logarithmic relationship between the excitation powder and PL intensity will be 1. Therefore, it is deduced that the slope between 1 and 2 can demonstrate the presence of TTA.
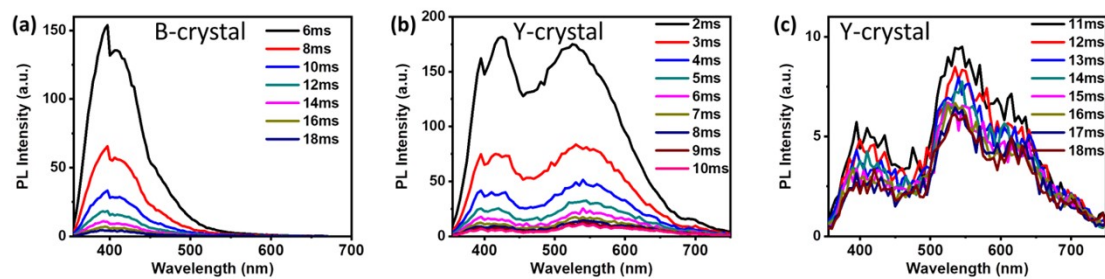
Figure S4. PL spectra of (a) B-crystal, (b) and (c) Y-crystal after different delayed times. A spectral fluctuation at ~400 nm was caused by instrument fluctuation.
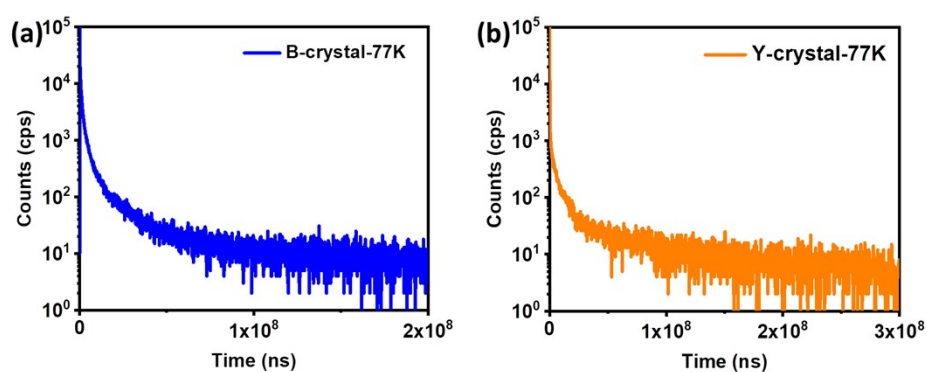
Figure S5. Time-resolved PL decay of (a) B-crystal and (b) Y-crystal for T_2 emission at 77 K.

For the B-crystal of IS-CBZ, after a long delayed time (Figure S4), a spectral redshift from λ_{max} = 398 nm to λ_{max} = ~406 nm was observed, and moreover, the lifetime at ~406 nm at 77 K became much larger than that at 398 nm at RT, demonstrating that a new emission band appeared at λ_{max} =~406 nm which should be originate from the T_2 state.
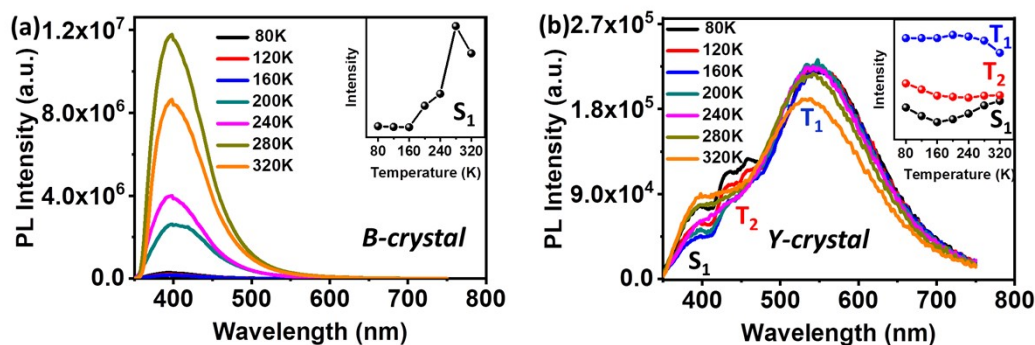
Figure S6. (a) Temperature-dependent PL spectra of (a) B-crystal and (b) Y-crystal, respectively.

To confirm the participation of T_2 state, the temperature-dependent PL spectra were measured from 80 K to 320 K for the Y-crystal. Once at 80 K, a new emission band appears around 438 nm with a long-lived lifetime of 71.1 ms (Figure S5), which is neither DF emission peaking at 398 nm nor phosphorescent emission from T_1 state peaking at 546 nm with a lifetime of 21.0 ms. This new emission band can be speculated to result from high-lying T_2 excited state. With increasing temperature, the intensity of T_2 emission peaking at 438 nm gradually decreases until it eventually disappears completely, while the DF emission peaking at 398 nm is enhanced from 160 K to 320 K (Figure S6). Therefore, the temperature-dependent PL spectra indicate a thermally activated up-conversion from T_2 to S_1 states in the case of a favorable $\Delta E_{S1-T2} = 0.29$ eV. Besides, the emission intensity of T_1 peaking at 546 nm keeps almost unchanged as the temperature increases from 80 K to 240 K, which reveals a compensation of T_1 exciton generation by internal conversion (IC) ($T_2 \rightarrow T_1$) process. To further verify the emission of T_2 state, the PL spectra of Y-crystal was measured with different delay times at 77 K (Figure S7). After a long delay time, both T_2 and T_1 emission can be clearly distinguished from S_1 emission peaking at 398 nm. At RT, the T_2 state is nonradiative due to temperature-accelerated quenching through two pathways of consumption: RISC ($T_2 \rightarrow S_1$) and IC ($T_2 \rightarrow T_1$).
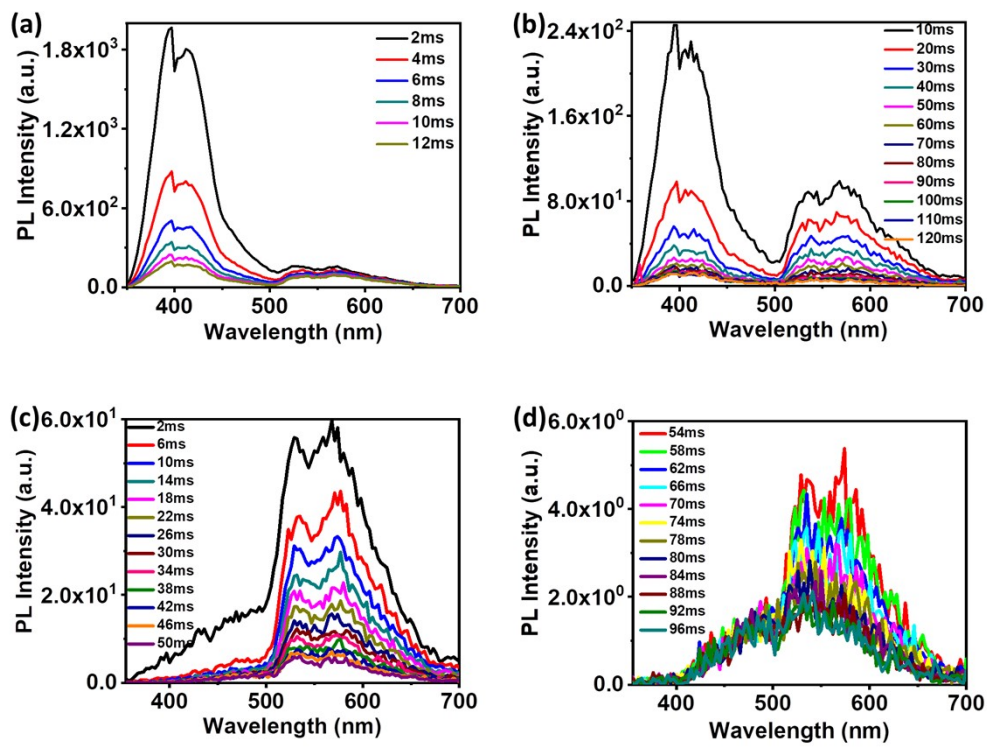
Figure S7. (a) and (b) PL spectra of B-crystal with different delay times at 77 K. A spectral fluctuation at ~400 nm was caused by instrument fluctuation. (c) and (d) PL spectra of Y-crystal with different delay times at 77 K.
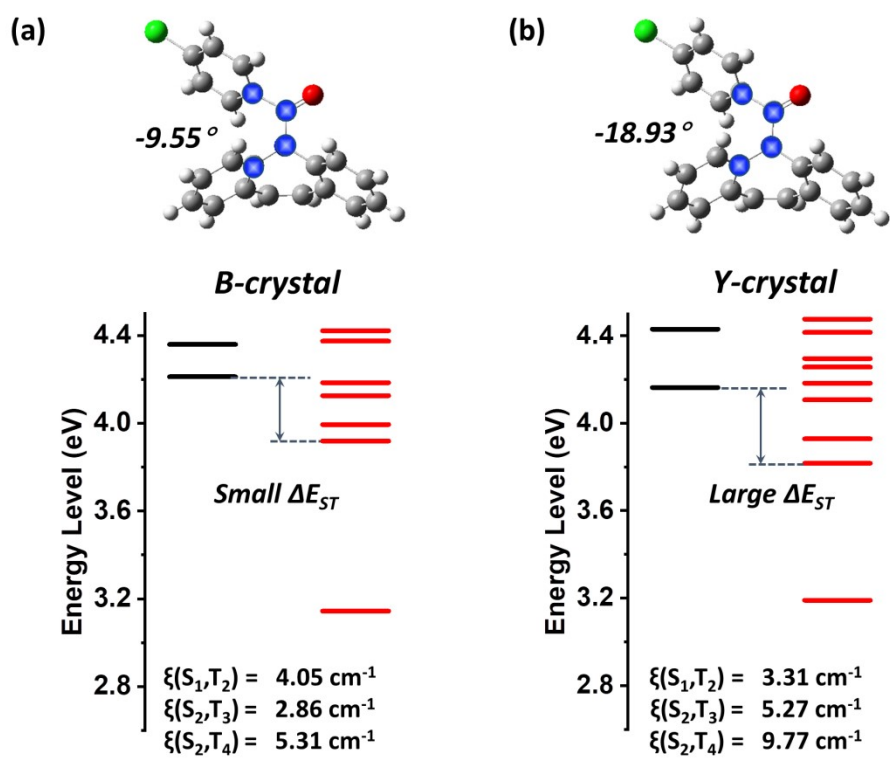
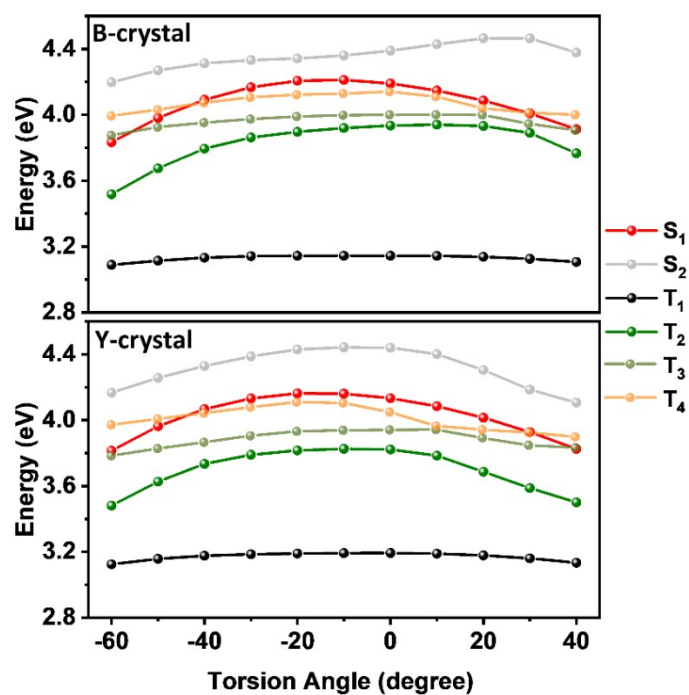**Figure S8.** Energy levels calculated from (a) B-crystal and (b) Y-crystal.

Figure S9. Theoretical simulation of energy levels versus twist angle θ between donor and acceptor from B-crystal and Y-crystal.

Theoretical energy levels as a function of θ between donor and acceptor demonstrate that $\Delta E_{S1\text{-}T2}$ shows a roughly shrinking trend as θ decreases (Figure S9). Exactly, IS-CBZ molecule has a larger θ in Y-crystal than that in B-crystal, leading to a relatively larger $\Delta E_{S1\text{-}T2}$ than that in B-crystal. This large $\Delta E_{S1\text{-}T2}$ reduces the reverse intersystem crossing (RISC) rate, and facilitates the generation of more triplet excitons for RTP occurence.
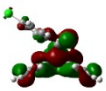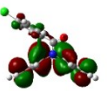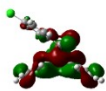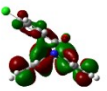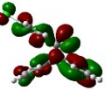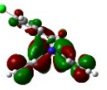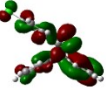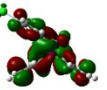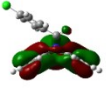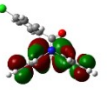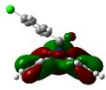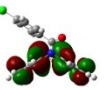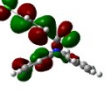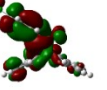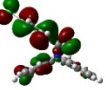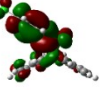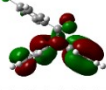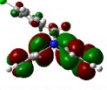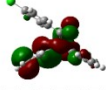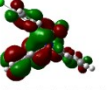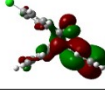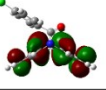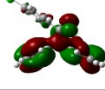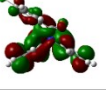
	B-crystal				Y-crystal		
S_1		98%	LE^1 (π, π^*)	S_1		98%	LE^1 (π, π^*)
S_2		93%	CT^1+LE^1 (n, π^*)	S_2		91%	CT^1+LE^1 (n, π^*)
T_1		93%	LE^3 (π, π^*)	T_1		92%	LE^3 (π, π^*)
T_2		75%	CT^3+LE^3 (n, π^*)	T_2		83%	LE^3 (n, π^*)
T_3		43%	LE^3 (n, π^*)	T_3		44%	CT^3+LE^3 (π, π^*)
T_4		85%	LE^3 (n, π^*)	T_4		83%	CT^3+LE^3 (π, π^*)

Figure S10. NTOs for B-crystal and Y-crystal. Molecular configurations are taken out directly from crystal structure.
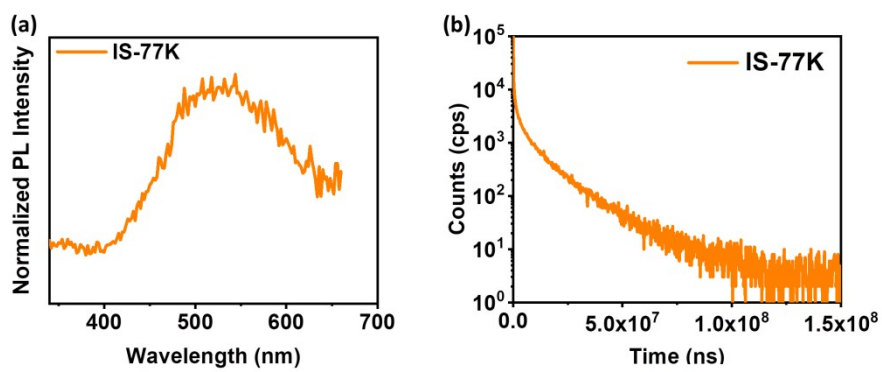
Figure S11. (a) Phosphorescence spectrum and (b) time-resolved PL spectrum at the maximum PL wavelength of IS in polymethyl methacrylate (PMMA) film carried out at 77 K.
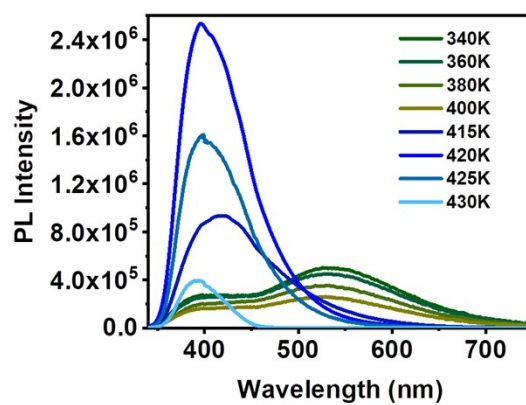
Figure S12. Temperature-dependent PL spectra of the ground samples.

Figure S13. The ^1H NMR (400 MHz, CD_2Cl_2, CF_3COOD, 25 °C, TMS) of IS-CBZ.

SI-3. Tables S1-S7

Table S1. Photophysical properties of different crystals under ambient conditions.

Samples	λ_{ML} (nm)	λ_F (nm)	λ_P (nm)	Φ_F (%)	Φ_P (%)
B-crystal	400	398	-	75.2	-
Y-crystal	-	398	546	1.4	6.7

Table S2. Bond lengths and twist angles of single-molecule conformations in the crystals

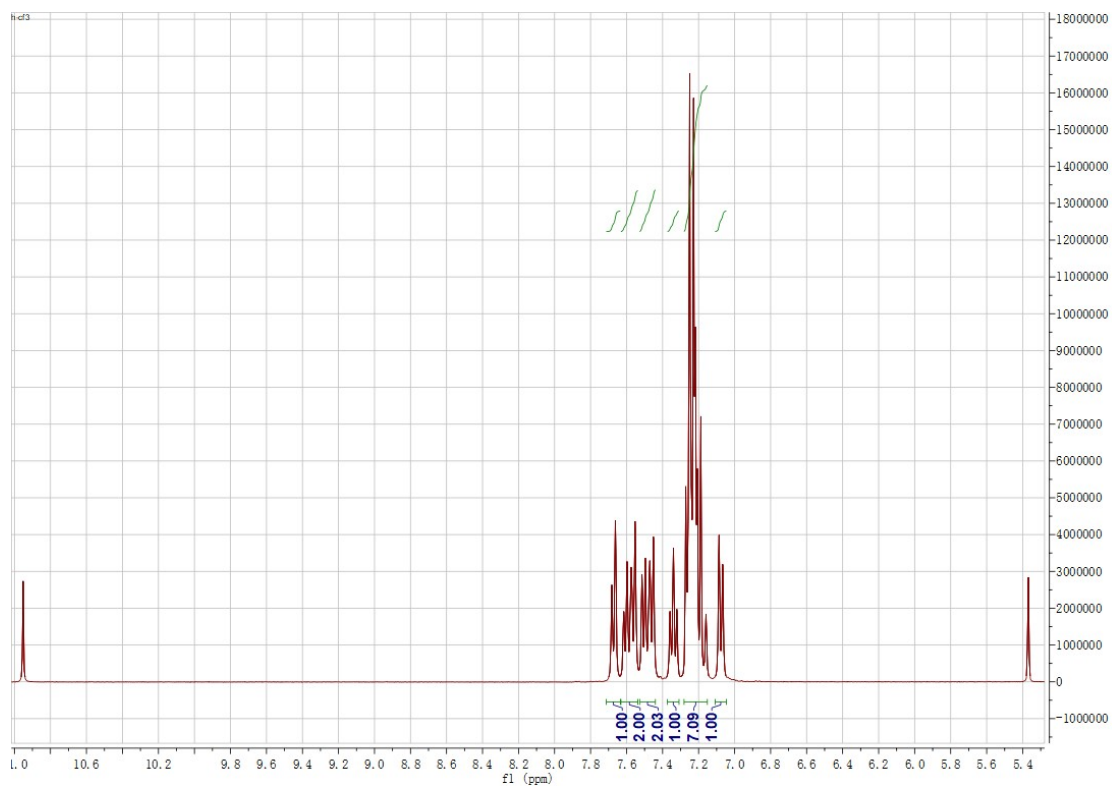| Samples	C1-C2	C2-N	C1-C2-O	O-C2-N	C3-N-C4	C1-C2-N-C3
B-crystal	1.503 Å	1.365 Å	120.99°	121.83°	115.27°	-9.55°
Y-crystal	1.501 Å	1.373 Å	120.93°	122.19°	115.17°	-18.93°

Table S3. Photophysical properties of two crystals at room temperature and 77 K.

Samples	τ_{PF} (ns)/τ_{DF} (µs)	τ_{RTP} (ms)	τ_P 77 K (ms)	τ_P 77 K (ms) of T_2
B-crystal	4.5/842.0	-	22.7	19.1
Y-crystal	3.3/ 808.3	2.1	21.0	77.1

Table S4. The SOC coefficients of IS-CBZ for B-crystal and Y-crystal. The unit of the SOC parameter is cm^{-1}.

Conformers	S_0-T_1	S_1-T_1	S_1-T_2	S_1-T_3	S_2-T_1	S_2-T_2	S_2-T_3	S_2-T_4
B-type	3.10	0.30	4.05	2.59	3.07	2.50	2.86	5.31
Y-type	3.49	0.53	3.31	2.18	3.23	1.44	5.27	9.77

Table S5. Crystallographic data of B-crystal and Y-crystal.

	B-crystal	Y-crystal
crystal color	colorless	colorless
empirical formula	$C_{21}H_{14}ONCl$	$C_{21}H_{14}ONCl$
formula weight	331.78	331.78
T [K]	293	293
crystal system	orthorhombic	triclinic
space group	P 21 c a	P -1
a [Å]	7.3045 (17)	9.7641 (3)
b [Å]	10.194 (3)	17.2051 (6)
c [Å]	22.727 (6)	9.8141 (4)
α [°]	90	90
β [°]	90	101.6015(14)
γ [°]	90	90
V [Å^3]	1692.2(7)	1615.01(10)
Z	1	1
F(000)	688	688
density [g/cm^3]	1.302	1.365
μ [mm^{-1}]	0.232	0.243
reflections collected	18791	16013
unique reflections	3774	7126
R (int)	0.0489	0.0175
GOF	1.092	1.042
R_1 [I>2σ(I)]	0.0549	0.0440
ωR_2 [I>2σ(I)]	0.0896	0.1078
R_1 (all data)	0.0853	0.0575
ωR_2 (all data)	0.0994	0.1168
CCDC	1967882	1967881

SI-4. References

1   M. J. Frisch, G. W. Trucks, H. B. Schlegel, G. E. Scuseria, M. A. Robb, J. R. Cheeseman, G. Scalmani, V. Barone, B. Mennucci, G. A. Petersson, H. Nakatsuji, M. Caricato, X. Li, H. P. Hratchian, A. F. Izmaylov, J. Bloino, G. Zheng, J. L. Sonnenberg, M. Hada, M. Ehara, K. Toyota, R. Fukuda, J. Hasegawa, M. Ishida, T. Nakajima, Y. Honda, O. Kitao, H. Nakai, T. Vreven, J. A. Montgomery, Jr., J. E. Peralta, F. Ogliaro, M. Bearpark, J. J. Heyd, E. Brothers, K. N. Kudin, V. N. Staroverov, T. Keith, R. Kobayashi, J. Normand, K. Raghavachari, A. Rendell, J. C. Burant, S. S. Iyengar, J. Tomasi, M. Cossi, N. Rega, J. M. Millam, M. Klene, J. E. Knox, J. B. Cross, V. Bakken, C. Adamo, J. Jaramillo, R. Gomperts, R. E. Stratmann, O. Yazyev, A. J. Austin, R. Cammi, C. Pomelli, J. W. Ochterski, R. L. Martin, K. Morokuma, V. G. Zakrzewski, G. A. Voth, P. Salvador, J. J. Dannenberg, S. Dapprich, A. D. Daniels, O. Farkas, J. B. Foresman, J. V. Ortiz, J. Cioslowski, and D. J. Fox, *Gaussian 09, Revision D.01,* Gaussian, Inc.: Wallingford CT, USA2009.

2   W. Liu, F. Wang and L. Li, *J. Theor. Comput. Chem.*, 2003, **2**, 257-272.

3   Z. Li, B. Suo, Y. Zhang, Y. Xiao and W. Liu, *Mol. Phys.*, 2013, **111**, 3741-3755.

4   Z. Li, Y. Xiao and W. Liu, *J. Chem. Phys.*, 2012, **137**, 154114.

5   Z. Li, Y. Xiao and W. Liu, *J. Chem. Phys.*, 2014, **141**, 054111.

6   A. Haefele, J. Blumhoff, R. S. Khnayzer and F. N. Castellano, *J. Phys. Chem. Lett.*, 2012, **3**, 299-303.